Flow past a sphere at the free-surface using URANS

Marion C. James*, Stephen R. Turnock, Dominic A. Hudson
Fluid-Structure Interactions Research Group; University of Southampton, Southampton, UK. SO17 1BJ

1 Introduction

A better understanding of the fluid-structure interactions of a sphere located at the free-surface would benefit many engineering fields such as the offshore oil and gas sector with storage tanks, the marine transportation industry with bulbous bows and submarines, as well as any swimming body. Most of these fields are within the Reynolds number range $4x10^4$ - $6x10^6$. Achenbach (1972) studied this Reynolds number range in a wind tunnel environment, and classified the different flow types observed into: sub-critical ($Re \leq 2x10^5$), critical ($2x10^5 \leq Re \leq 4x10^5$), super-critical ($4x10^5 \leq Re \leq 10^6$) and transcritical ($Re \geq 10^6$). Hoerner (1965) gathered several experimental data, and identified that the drag coefficient has a fairly constant value of 0.47 at sub-critical Reynolds numbers, but it drops drastically to a value of 0.1 between $2x10^5$ and $4x10^5$. This phenomenon is well known under the name of 'drag crisis'. As the flow speed increases, mixing of the turbulences becomes more chaotic in the boundary layer region increasing the fluid momentum. Consequently, the boundary layer flow separation is delayed resulting in a decrease in the pressure differential between the front and the rear of the sphere.

The critical Reynolds number range was further studied experimentally by Taneda (1978), Jeon et al. (2004), Bakic and Peric (2005), Ozgoren et al. (2011). Taneda (1978) identified separation points using an oil-flow visualisation technique. On average, the flow separates at an angle of 80°from the front stagnation point for $10^4 \leq Re \leq 3x10^5$. Furthermore, Taneda (1978) observed a radical change in the boundary layer characteristics around $Re = 3.5x10^5$ with three speration lines at 100°, 117°and 135°. These lines may be identified as the laminar separation line, the reattachment line and the turbulent separation line respectively. At the rear of the sphere, an Ω -shaped line was observed due to the reattachment of all the streamlines. Hair-pin vortices are shed at the rear of the sphere in an asymmetric manner (Kiya et al., 2000). Bakic et al. (2006) underlined the complexity of the wake structure behind the sphere and identified the existence of a sub-harmonic of the vortex shedding frequency.

Only a few numerical investigations of the flow past a sphere have been performed to-date. Large-Eddy Simulations (LES) and Detached-Eddy Simulations (DES) were undertaken at sub-critical (Constantinescu, 2000) and supercritical (Jindal et al., 2004) Reynolds numbers. Good agreements with experimental data gathered by Achenbach (1972) were found for the drag coefficient and the pressure distribution.

The influence of the free-surface on a submerged sphere travelling at a speed equivalent to Reynolds number 5000 was studied both experimentally and numerically ((Hassanzadeh et al., 2012), (Ozgoren et al., 2012), (Ozgoren et al., 2013)). For small immersion depths, Hassanzadeh et al. (2012) showed that the recirculating region in the half-lower side of the wake region is larger compared to the half-upper side. Furthermore, a strong interaction between the fluctuated streamwise and transverse velocities in the half-lower side of the wake region was observed leading to a higher mixing flow rate. A strong interference between the sphere wake and the free-surface was noticed by Ozgoren et al. (2013) at an immersed depth to diameter ratio of 0.25 (from the top side of the sphere). However, no literature on the fluid-structure interactions of a sphere located at the free-surface is known by the author, as previously mentioned by Ozgoren et al. (2012).

Consequently, this paper will investigate the influence of the free-surface on the flow past a sphere located half-way between the air and water phases using Unsteady Reynolds-Averaged Navier-Stokes (URANS) simulations, and validated with experimental data obtained in a towing tank environment.

2 Towing Tank Experiment

The flow past a sphere located at the free-surface, was studied over the critical Reynolds number range: $2x10^5 \leq Re \leq 4x10^5$. Experiments were carried out in the Lamont tank at the University of Southampton. The tank dimensions are: 30 x 2.4 x 1.2 $[m^3]$. The equivalent depth-based Froude number for the tested speeds is between 0.3 and 0.7 (ie. within the sub-critical flow range).

Due to time and cost constraints, a first sphere prototype was manually constructed based on a youth-size basketball covered with an epoxy resin. The resulting sphere diameter is 225mm and was

** *corresponding author's e-mail*: M.James@soton.ac.uk

ballasted in order to attain neutral buoyancy. Drag measurements were taken at speeds between 1.0 and 2.2 $m.s^{-1}$ with a 0.2 $m.s^{-1}$ step, and further data points were obtained around the transitional point. The water temperature was recorded as 10 degrees Celsius, thus the kinematic viscosity value was taken as $1.31\text{x}10^{-6} m^2.s^{-1}$ (Newman, 1977).

An above-water camera was placed on the carriage in order to identify the separation angle. Drag and side forces were both recorded. Digital signal processing of the side force trace was performed to determine the shedding frequency of the vortex street formed at the rear of the sphere at high Reynolds numbers. The power spectral distribution was evaluated using the 'PWELCH' function in Matlab for each speed and for a sampling frequency of 100 Hz. This function is based on the Goertzel algorithm which efficiently solves the coefficients from the discrete Fourier transform in order to get the sampling data from the time domain into the frequency domain (Roth, 2008).

The vortex shedding frequency was identified from the power spectral distribution. This frequency represents the number of vortices formed at one side of the 'street' in the unit of time (Hoerner, 1965). The non-dimensionalised form is commonly called Strouhal number and may be expressed as $St = \frac{F_S D}{V}$.

Furthermore, an array of two wave probes was positioned on the side of the tank to obtain the wave resistance created by the sphere. A labelled picture of the experimental set-up is provided in Figure 1.

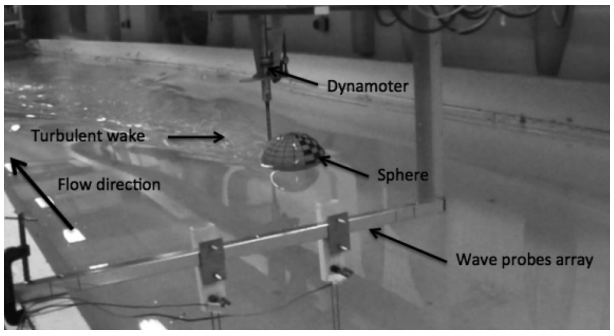

Figure 1: Overview of experiment set-up in the Lamont tank (University of Southampton)

3 Numerical Investigation

Due to time constraints, the experimental study only covered the case of a sphere located at the free-surface. The influence of the sphere's immersion depth on wave resistance was first analysed using a linear potential flow theory, before solving the Navier-Stokes equations.

3.1 Potential flow

Early linear potential flow method was pioneered by Michell (1898) and Eggers (1955), and further developed by Insel (1990) in order to determine the wave pattern of slender bodies and their associated wave resistance through a homogeneous, inviscid, incompressible and irrotational flow. The disturbance velocity potential of the discretised body is assumed to be generated by a distribution of Havelock sources over the centreline of the body (y = 0). According to Michell (1898), these sources have a strength of magnitude 2*U*Y(x,z), where U is the free stream velocity and Y(x,y) the offset at point (x,z). Couser et al. (1998) improved the results obtained from Insel (1990) method with the addition of a virtual appendage to the hull transom. The separated flow at low speeds and the air cavity at high speeds were then accounted for.

The wave resistance of the sphere tested in the Lamont tank was evaluated using an in-house potential flow code. The domain was defined by the Lamont tank width and depth dimensions (2.4 x 1.2 $[m^2]$). The sphere was discretised with 4900 triangular panels (50 vertical faces and 50 around faces). A virtual cylinder was then added at the rear of the sphere in order to simulate the separated wake at the lower speeds and the air gap at the higher speeds. Only the front half of the sphere was kept with the same level of discretisation and a cylinder of base D and height 2.5D (where D is the sphere diameter) was added (Figure 2).

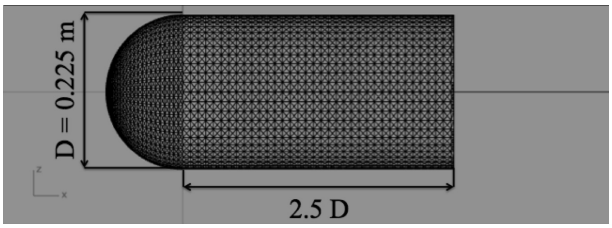

Figure 2: Discretised sphere and virtual appendage added to model the separated flow at low speeds

The effect of the virtual appendage on the total resistance was studied for the sphere located at the free-surface and compared with the experimental data. Based on these findings (Section 4.2), the influence of immersion depth on the wave resistance was tested across the critical Reynolds number range. The immersion depth of the sphere may be compared to the draught of a ship (i.e. the distance between the bottom of the sphere and the free-surface). It will be expressed as a percentage of the sphere diameter throughout this report.

3.2 URANS simulations

3.2.1 Pre-processing

The domain size is matched to the Lamont tank with both water and air phases separated by a free-surface. The cross-sectional area is based on the Lamont tank width and depth (2.4 x 1.2 $[m^2]$) in order to replicate the same blockage. An air draught of four sphere diameters above the free-surface was chosen. The air draught is thought to not have much influence on the results since the air resistance is considered as negligible. The domain total length is 3.2m, allowing 3D upstream and 10D downstream of the sphere.

Boundary conditions were chosen to closely represent the experimental conditions. The velocity and pressure fields inlet and outlet boundary conditions are fixedValue/outletInlet and zeroGradient/fixedValue respectively. The turbulence model entry fields (k, omega, nut) have fixed inlet values and zero gradient outlet boundary conditions. The sphere is modelled as a non-slip wall and the sides are considered as slip to reduce the computational time.

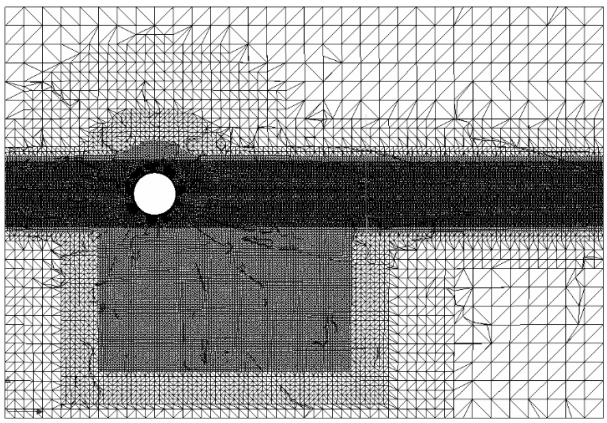

Figure 3: Hybrid mesh in the x-z plane

The OpenFOAM meshing tool snappyHexMesh (2.1.1) was used to design a hybrid mesh. A structured boundary layer was built on the sphere with a y^+ value of 30, based on the turbulent boundary layer thickness defined by Newman (1977). A non-structured mesh surrounds the sphere across the entire domain. The refined mesh at the free-surface was constructed to accommodate twice the wave elevation recorded during the experiment. The free-surface mesh was further refined vertically to effectively capture the wave pattern. Furthermore a refinement box was added around the sphere (1D upstream, 4D downstream) in order to define the stagnation point correctly and take into account the high pressure gradients just upstream of the sphere and in the wake. Using a smooth growth rate throughout the domain, a numerical beach was added at the outlet to damp any waves which may be reflected. This mesh design totals 3.4 million cells and is shown in Figure 3.

3.2.2 Simulation

Due to the inclusion of a free-surface, the solver interFoam (version OF-2.2.0) was used to simulate the flow past the sphere with a Courant number of 1.2 to allow the simulations to run faster without compensating on the results' accuracy. The turbulence model $k\omega - SST$ was applied since it accurately models boundary layers under strong adverse pressure gradients, separation and recirculation. The turbulent energy, dissipation rate and viscosity were respectively defined as follows: $k = \frac{3}{2}(UI)^2$, $\omega = C_\mu^{-\frac{1}{4}}$, $\nu_T = \sqrt{\frac{3}{2}}(UIL)$.

A turbulence intensity of 1% was selected, although an investigation on the influence of the turbulence intensity level on the results should be performed. The turbulent length scale was based on 0.07D and the usual turbulent constant of 0.09 was used.

The sphere was first located three diameters below the free-surface and progressively brought up to the free-surface. The internal fields of the case with the sphere at the free-surface were mapped with a case where the sphere had one diameter of immersion depth to allow smooth formation of the wave pattern.

4 Results and Discussion

4.1 Qualitative results

From the above-water camera positioned above the sphere, screenshots were taken at each speed. A matrix of these screenshots is presented in Figure 4. It may be noticed that the flow stays laminar up to a speed of 1.7 $m.s^{-1}$ (Re = 2.9 x 10^5), and then transitions to turbulent at 1.75 $m.s^{-1}$ (Re = 3.0 x 10^5). After transition, the sphere wetted surface area is maximal, and as speed increases the flow stays attached to the sphere for longer reducing the pressure differential between the front and the rear of the sphere and hence decreasing the pressure drag. The transition from laminar to turbulent flow is strongly influenced by the free-surface with the creation of a bow wave at the lower speeds. The resulting flow characteristics should be further investigated with the use of dye paint and pressure sensors.

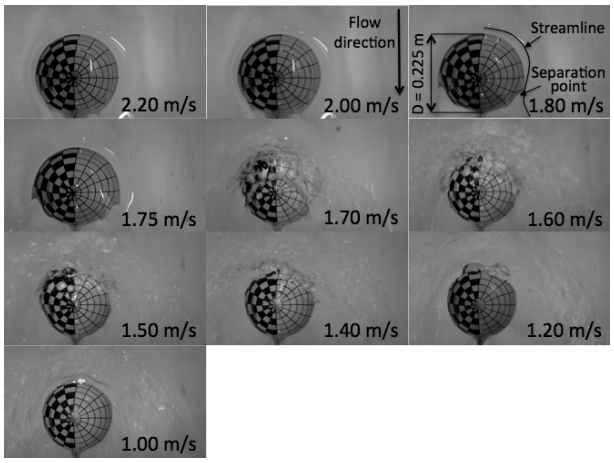

Figure 4: Above water screenshots emphasising transition from laminar to turbulent flow

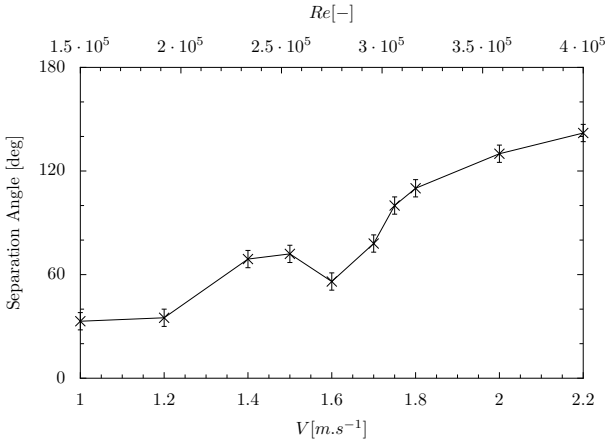

Figure 5: Separation angle versus speed measured from above camera (+/- 5 degrees error margin)

From Figure 4, the separation angle was measured to study the variation with speed (Figure 5). At the lowest speed, a separation angle of 35°was found although this is suspected to be an observation of the bow wave characteristic. The separation angle increased up to about 70°just before the transitional speeds and reached 142°at 4x10^5.

4.2 Drag force

Figure 6 provides a comparison of the total resistance coefficient obtained experimentally, with potential flow and from CFD simulations for a sphere advancing at the free-surface with speeds ranging between 1.0 $m.s^{-1}$ and 2.2 $m.s^{-1}$.

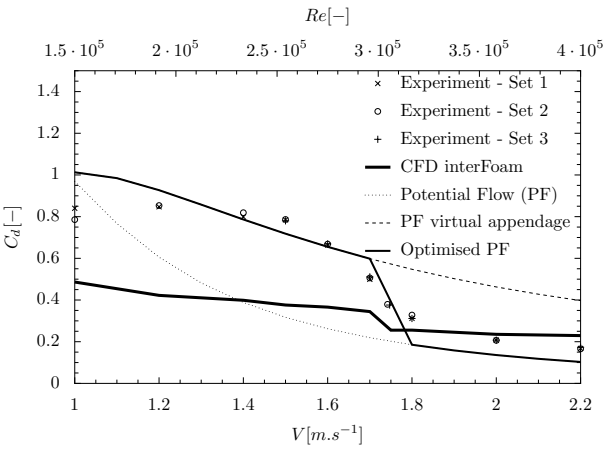

Figure 6: Comparison of resistance curves obtained from the experiment, potential flow and CFD

During the towing tank tests, the drag force was recorded using a sampling frequency of 100 Hz. The drag force was averaged over the steady portion of the drag force trace and non-dimensionalised with $0.5\rho A_p V^2$. Three repeats for each speed were performed in order to obtain an accurate mean drag curve as shown in Figure 6. The repeatability of the results proved to be very good, with a maximum error of 6.5% at the lowest speed and on average only a 0.5% discrepancy was recorded. At the lower speeds (below Re = 2.6 x 10^5), a constant drag coefficient of 0.8 was measured. The drag crisis follows between 1.5 $m.s^{-1}$ and 2.0 $m.s^{-1}$, and the drag coefficient drops down to 0.17 at 2.2 $m.s^{-1}$ (Re = 3.8 x 10^5).

Potential flow applied to the sphere only underpredicts the wave resistance and thus the total drag. The drag curve for the sphere including the virtual cylinder appendage is also displayed in Figure 6. At low speeds, there appears to be a better match with the experimental data for the sphere with the virtual appendage. Indeed, the flow separates early on after the stagnation point as emphasised in Figure 4. However, at higher speeds, there is a better agreement on the drag coefficient between experimental data and potential flow for the sphere without the virtual cylinder attached. Figure 7 exhibits a flow which stays attached to the sphere over a long portion of the sphere at the maximum speed tested. This translates in a very narrow (or absent) air cavity at the rear of the sphere, cancelling the need for a virtual appendage.

CFD simulations largely underestimate the drag coefficient at the laminar speeds. It is important to note that, due to time constraints, the mesh designed for a speed of 2.0 $m.s^{-1}$ was used for all tested speeds and may therefore not be adapted to the laminar speeds. Furthermore, all laminar speeds were run with the $k\omega - SST$ turbulence models. It would be preferable to re-run these sim-

ulations with the laminar RASmodel, acting as a dummy turbulence model.

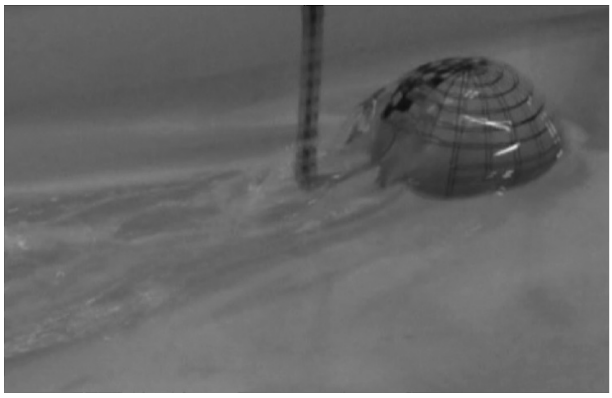

Figure 7: Turbulent wake at Re = 3.8 x 10^5

4.3 Shedding frequency analysis

Strouhal number obtained from the experiment is plotted in Figure 8 and compared with Hoerner (1965) empirical formula ($St = \frac{0.21}{(C_d)^{\frac{3}{4}}}$) for fully submerged bluff bodies. Before transition, there is a large discrepancy between Strouhal number from the experiment and from Hoerner (1965). A bow wave is indeed created at the lower speed and early separation occurs as previously observed in Figure 4. The wetted surface area of the sphere is thus less than when fully submerged. However, after transition, the wetted surface area is maximal and the sphere may now be considered to be in a similar condition as a fully submerged sphere since it sits just under the bow wave. Indeed, Strouhal number at the highest speed (2.2 $m.s^{-1}$) tends towards the empirical formula defined by Hoerner (1965) (Figure 8).

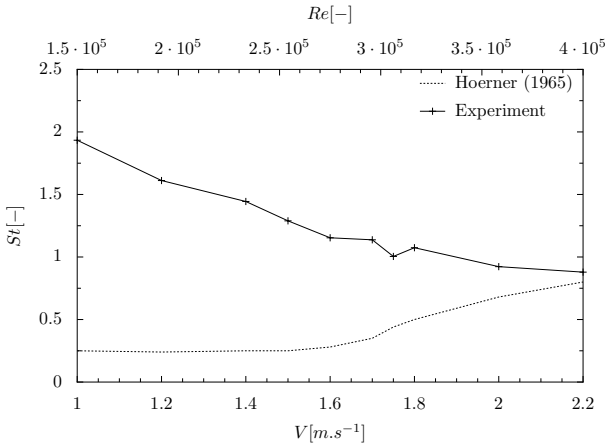

Figure 8: Strouhal number versus speed

4.4 Influence of immersion depth and speed

Due to time constraints, the experimental study only covered the case of a sphere located at the free-surface. The influence of the sphere's immersion depth on wave resistance was therefore first analysed using a linear potential flow theory. Based on previous findings (Figure 6), at speeds between 1.0 $m.s^{-1}$ and 1.7 $m.s^{-1}$, the virtual cylinder was added; and, above 1.7 $m.s^{-1}$, only the sphere was modelled.

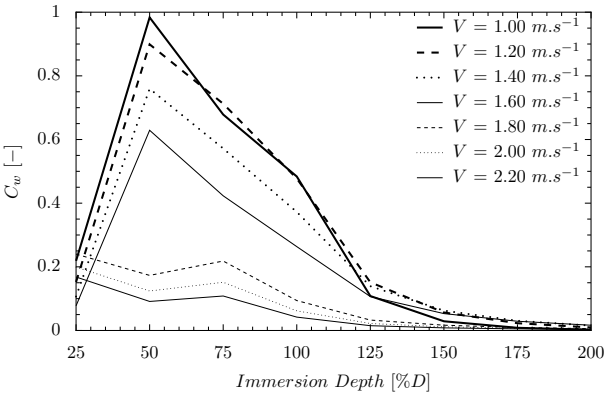

Figure 9: Influence of the sphere's immersion depth on the wave resistance across a range of Re (1.7x10^5 to 3.8x10^5) using potential flow theory

Figure 9 illustrates that maximum wave resistance occurs when the sphere is half-submerged as a consequence of the maximum cross-sectional area being at the free-surface. Wave resistance decreases sharply when the sphere has an immersion depth equal to 125% D, and becomes negligible as the sphere reaches an immersion of 175% D. As speed increases, the wave resistance coefficient decreases due to delayed separation and reaches a peak value at immersion depth 25% D and 75% D. Further data points would be needed when the sphere is partially submerged.

5 Conclusions and Further Work

In this paper, it was confirmed that the free-surface has a strong influence on the flow past a sphere at critical Reynolds numbers. Indeed, the drag coefficient doubles at low speeds compared to single phase problems due to the energy dissipation through the distortion of the free-surface. The drag crisis was observed for 2.5x10^5 $\leq$ Re $\leq$ 3.4x10^5.

The use of a virtual appendage at laminar speeds proved to be effective when using a potential flow method.

Initial results from URANS simulations agree with the experiment at turbulent Reynolds num-

bers; however an investigation of different turbulence models should be undertaken at speeds before the drag crisis. Furthermore, Large-Eddy Simulations (LES) should be performed in order to better capture the unsteadiness of the vortex shedding.

Maximum wave resistance occurs when the sphere is half-submerged due the maximum cross-sectional area of the sphere. The wave resistance component becomes negligible at an immersion depth greater than 175%D.

References

Achenbach, E. (1972), 'Experiments on the flow past spheres at very high Reynolds numbers', *Journal of Fluid Mechanics* **54**(03), 565.

Bakic, V. and Peric, M. (2005), 'Visualisation of flow around sphere for Reynolds numbers between 22000 and 400000', *Thermophysics ad Aeromechanics* **12**(3), 307–315.

Bakic, V., Schmid, M. and Stankovi, B. (2006), 'Experimental investigations of turbulent structures', pp. 97–112.

Constantinescu, G. S. (2000), 'LES and DES investigations of turbulent flow over a sphere', *AIAA Journal* **0540**, 1–11.

Couser, P. R., Wellicome, J. F. and Molland, A. F. (1998), 'An improved method for the theoretical prediction of the wave resistance of transom-stern hulls using a slender body approach', *International Shipbuilding Progress* **45**(444), 1–18.

Eggers, K. (1955), 'Resistance components of two-body ships', *Jahrbuch der Schiffbautechnischen Gesellschaft,* **49**.

Hassanzadeh, R., Sahin, B. and Ozgoren, M. (2012), 'Large eddy simulation of free-surface effects on the wake structures downstream of a spherical body', *Ocean Engineering* **54**, 213–222.

Hoerner, S. F. (1965), *Fluid-dynamic drag*, Hoerner Fluid Dynamics.

Insel, M. (1990), An investigation into the resistance components of high speed displacement catamarans, PhD thesis, University of Southampton.

Jeon, S., Choi, J., Jeon, W.-P., Choi, H. and Park, J. (2004), 'Active control of flow over a sphere for drag reduction at a subcritical Reynolds number', *Journal of Fluid Mechanics* **517**, 113–129.

Jindal, S., Long, L. N. and Plassmann, P. E. (2004), Large eddy simulations around a sphere using unstructured grids, *in* '34th AIAA Fluid Dynamics', Vol. 7, pp. 1–16.

Kiya, M., Mochizuki, O. and Ishikawa, H. (2000), Challenging issues in separated and complex turbulent flows, *in* '10th International Symposium on Applications of Laser Techniques to Fluid Mechanics', Lisbon, Portugal, pp. 1–13.

Michell, J. H. (1898), 'The wave-resistance of a ship', *Phil. Mag.* **45**(5), 106–123.

Newman, J. N. (1977), *Marine Hydrodynamics*, The Massachussets Institute of Technology.

Ozgoren, M., Dogan, S., Okbaz, A., Aksoy, M. H., Sahin, B. and Akilli, H. (2013), 'Comparison of flow characteristics of different sphere geometries under the free surface effect', *EPJ* **45**.

Ozgoren, M., Dogan, S., Okbaz, A., Sahin, B. and Akilli, H. (2012), 'Passive control of flow structure interaction between a sphere and free-surface', *EPJ* **25**.

Ozgoren, M., Okbaz, A., Kahraman, A., Hassanzadeh, R., Sahin, B., Akilli, H. and Dogan, S. (2011), Experimental investigation of the flow structure around a sphere and its control with jet flow via PIV, *in* '6th IATS', number 5, pp. 16–18.

Roth, E. H. (2008), Artic Ocean long-term acoustic monitoring: ambient noise, environmental correlates, and transients North of Barrow, PhD thesis, University of California, San Diego.

Taneda, S. (1978), 'Visual observations of the flow past a sphere at Reynolds numbers between 10^4 and 10^6', *Journal of Fluid Mechanics* **85**(1), 187 – 192.